Available online at www.sciencedirect.com
ScienceDirect
Trans. Nonferrous Met. Soc. China 22(2012) 2813−2821
Transactions of Nonferrous Metals Society of China
www.tnmsc.cn

Removal of SiC particles from solar grade silicon melts by imposition of high frequency magnetic field

Mehdi KADKHODABEIGI[1], Jafar SAFARIAN[1], Halvard TVEIT[1], Merete TANGSTAD[1], Stein Tore JOHANSEN[2]

1. Department of Materials Science and Engineering, Norwegian University of Science and Technology (NTNU), P.O. Box 7491, Trondheim, Norway;
2. SINTEF Materials and Chemistry, Flow Technology Group, P.O. Box 7465, Trondheim, Norway

Received 8 December 2011; accepted 8 April 2012

Abstract: Non-metallic particles and metallic impurities present in the feedstock affect the electrical and mechanical properties of high quality silicon which is used in critical applications such as photovoltaic solar cells and electronic devices. SiC particles strongly deteriorate the mechanical properties of photovoltaic cells and cause shunting problem. Therefore, these particles should be removed from silicon before solar cells are fabricated from this material. Separation of non-metallic particles from liquid metals by imposing an electromagnetic field was identified as an enhanced technology to produce ultra pure metals. Application of this method for removal of SiC particles from metallurgical grade silicon (MG-Si) was presented. Numerical methods based on a combination of classical models for inclusion removal and computational fluid dynamics (CFD) were developed to calculate the particle concentration and separation efficiency from the melt. In order to check efficiency of the method, several experiments were done using an induction furnace. The experimental results show that this method can be effectively applied to purifying silicon melts from the non-metallic inclusions. The results are in a good agreement with the predictions made by the model.

Key words: SiC particle; electromagnetic separation; solar grade silicon (SoG-Si); photovoltaic cells; computational fluid dynamics (CFD); non-metallic particles; metallic impurities

1 Introduction

Carbothermic reduction of quartz in submerged arc furnaces is the established process in order to produce metallurgical grade silicon (MG-Si). The liquid silicon produced at temperatures around 2000 °C contains dissolved carbon. After tapping the melt from the furnace, additional SiC particles will be formed, as the solubility of carbon in liquid silicon decreases with falling the temperature [1].

One of the important applications of silicon is in making of photovoltaic solar cells. Existence of SiC particles in the solidified silicon can cause shunting in the solar cells as well as affecting the mechanical properties of the cells. Therefore, these inclusion particles must be removed from the silicon melt before solar cells are fabricated.

Electromagnetic processing of materials (EPM) has been widely applied to the continuous casting of steel like electromagnetic stirring and electromagnetic braking for the purpose of clean steel production [2]. Recently, effective separation methods of non-metallic inclusions from liquid steel have been more searched because of the strong demand for higher cleanliness of steel products. Concerning nonferrous metals like aluminium and copper, the situation is the same. Especially for recycling of aluminium, fine inclusions from molten scrap must be removed. Electromagnetic (EM) separation based on the works done by LEENOV and KOLIN [3] and MARTY and ALEMANY [4], is one of the most promising methods for inclusion removal. Various methods have been proposed to generate EM forces in liquid metals: imposition of alternating current [5], simultaneous imposition of alternating current and AC magnetic field [6,7] and imposition of AC magnetic field [8−10].

It is well known that silicon has a quite low electrical conductivity (σ_s=5×10^4 S/m) in the solid phase. However, liquid silicon has an electrical conductivity of σ_m=1.23×10^6 S/m, which is approximately twenty five times more than the solid conductivity [11]. Such high electrical conductivity of the silicon melt makes it possible to remove the nonconductive inclusions from the melt using electromagnetic separation method. In the

Corresponding author: Mehdi KADKHODABEIGI; E-mail: mehdi.kadkhodabeigi@material.ntnu.no
DOI: 10.1016/S1003-6326(11)61537-9

current research, the feasibility of electromagnetic separation method for removal of SiC particles from silicon melt is studied.

2 Principle of electromagnetic separation

According to Leenov-Kolin's theory [3], when a uniform electromagnetic force is applied to a liquid metal, the metal is compressed by the electromagnetic force and a pressure gradient is generated in the metal. The nonconductive particles in the liquid metal receive only pressure because they do not experience the electromagnetic force. This phenomenon is simply shown in Fig. 1.

LEENOV and KOLIN [3] derived a theoretical expression of the force acting on a single sphere suspended in liquid metal in the case that the electrical conductivities of the sphere (σ_p) and liquid (σ_L) are different. The equation is

$$\boldsymbol{F}_p = -\frac{3}{2}\cdot\frac{\sigma_L-\sigma_p}{2\sigma_L+\sigma_p}V_p\boldsymbol{F} \tag{1}$$

where $\boldsymbol{F}_p$ is the separation force acting on a sphere; V_P is the volume of the sphere and $\boldsymbol{F}$ is the electromagnetic force (EMF) given by:

$$\boldsymbol{F} = |\boldsymbol{J}\times\boldsymbol{B}| \tag{2}$$

where $\boldsymbol{J}$ is the induced current density; $\boldsymbol{B}$ is the magnetic flux density.

This separation force does not include the effect of fluid flow around the spherical particle because the viscous force cancels out totally on the sphere. As the inclusion particles are nonconductive compared with the liquid metal in general, σ_p is zero in Eq. (1) and the following equation is obtained:

$$\boldsymbol{F}_p = -\frac{3}{4}\cdot\frac{\pi d_p^3}{6}\boldsymbol{F} \tag{3}$$

where d_p is the particle diameter.

In the case where the AC magnetic field is imposed alone, the induced electromagnetic force should be restricted in a skin depth given by the following equation:

$$\delta = \frac{1}{\sqrt{\pi f\mu_L\sigma_L}} \tag{4}$$

where μ_L is the relative liquid permeability.

The skin depth becomes thin with increasing the frequency, f. In order to enhance the separation, the mean convection velocity and turbulent dissipation are effective to carry particles from the bulk of liquid to the vicinity of the wall, where a strong electromagnetic force captures them. Using the physical properties of the silicon melt (Table 1) and frequency of the induction furnace (Table 2), the skin depth δ is equal to about 4.33 mm.

Table 1 Physical properties of silicon melt and SiC particles [11,12]

Material	Density/ ($kg\cdot m^{-3}$)	Electrical conductivity/ ($S\cdot m^{-1}$)	Viscosity/ ($Pa\cdot s^{-1}$)	Melting point/°C
Silicon (melt)	2560	1.23×10^6	0.00075	1415
SiC	3185	0.0001−1	−	2735

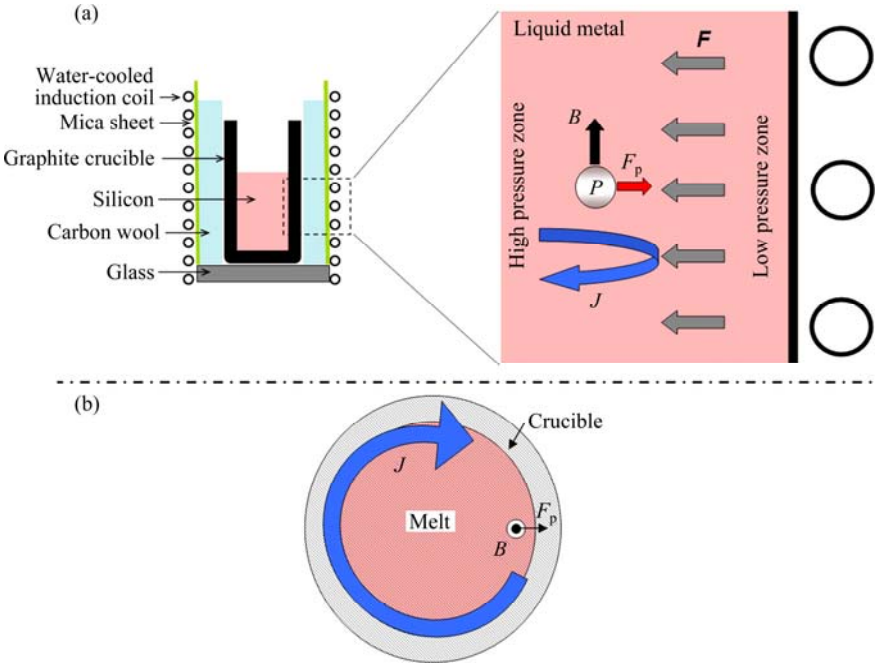

Fig. 1 Graphical presentation of principle behind electromagnetic separation of nonconductive inclusions from liquid metals (a) and electromagnetic forces inserted on particle in cross section of melt (b)

Table 2 Geometrical and electrical parameters of induction furnace

Coil diameter/cm	Coil length/cm	Coil electric current/A	Power frequency/Hz	Coil turns number
10.0	15.0	385	11000	10

3 Experimental

In order to check the separation of SiC particles from molten silicon under electromagnetic forces, induction melting of silicon containing SiC particles was done.

3.1 Material

Industrial metallurgical grade silicon (MG-Si) with the particle size in the range of 1−5 mm was used in the present study as the main material. Physical properties of silicon melt and SiC particles are given in Table 1 [11,12]. Silicon carbide particles with the average particle size of 9 μm (Fig. 2) were melted with the silicon and Si/SiC composites containing 3% and 10% SiC were produced. Inside the graphite crucible and close to the melting point of silicon, SiC particles exist in the melt as a separate phase. These composites were crushed down to 1 mm and added to MG-Si in four experiments, as listed in Table 3.

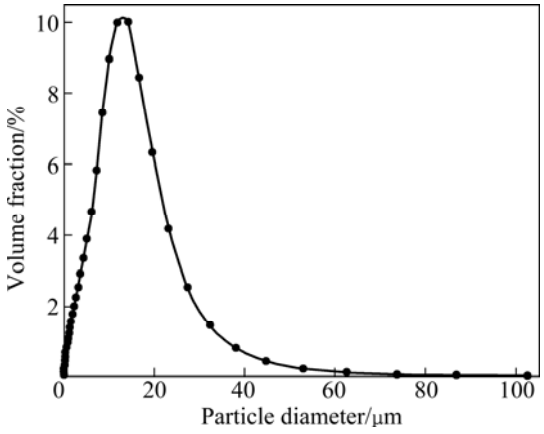

Fig. 2 Size distribution of SiC particles

Table 3 Amount and composition of silicon materials

Experiment No.	*m*(Si/SiC)/g	*m*(MG-Si)/g	Total SiC content in melt/%
A	1.73 *	128.2	0.04
B	14.3 *	128.5	0.3
C	14.4*	130	0.3
D	12.8**	128.4	1.0

* 3% SiC, ** 10% SiC

Silicon and Si/SiC composite were put in a graphite crucible prepared from dense graphite (Carbone Lorraine 2020) with dimensions of 100 mm in height, 50 mm in outside diameter and 40 mm in inside diameter. The material charge was distributed in two different ways for the experiments as schematically shown in Fig. 3.

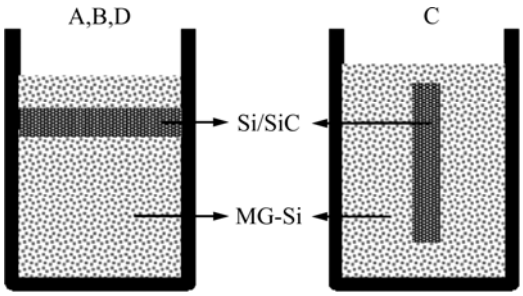

Fig. 3 Material charge in graphite crucible for experiments A to D

3.2 Induction melting

The induction melting of the material was done in a vacuum induction furnace with the coil dimensions listed in Table 2. The furnace chamber was evacuated two times with a mechanical pump to below 0.1 Pa followed with Ar (99.999%) flashing. The melting was then carried out under continuous Ar flow. The furnace power was tuned in the way to be enough to keep the melt temperature of 150 g silicon around 1450 °C where the melt surface temperature was recorded by a portable pyrometer.

The melting of material was possible to be observed from a glass window on the furnace top. The melting was completed in about 12 min and then the power was tuned to keep the melt temperature close to the silicon melting point. Then melt was held at constant temperature for 12 min. The crucible was then cooled down through power off and silicon was solidified in the crucible. It is found that for all experiments the solidification starts from the top of the melt and completes at the bottom, resulting in cracks in the graphite crucible bottom due to the silicon expansion through solidification.

3.3 Metallography

The crucibles containing the solidified silicon were cut vertically from the middle by a diamond cutter and metallography samples were then prepared. The distribution of silicon carbide particles were studied by microscopy and micrographs were used as documentation.

4 Mathematical modelling

As discussed above, the electromagnetic forces will cause segregation of the inclusion particles from the liquid metal. The segregation rate is obtained easily as a product of the particle concentration (uniform) and the

migration velocity due to electromagnetic force perpendicular to the side wall and the bottom. Expressing the migration velocities based on the forces exerted to the particles is an essential step of explaining the segregation procedure. Figure 4 shows the different forces and migration velocities for a single particle in the melt.

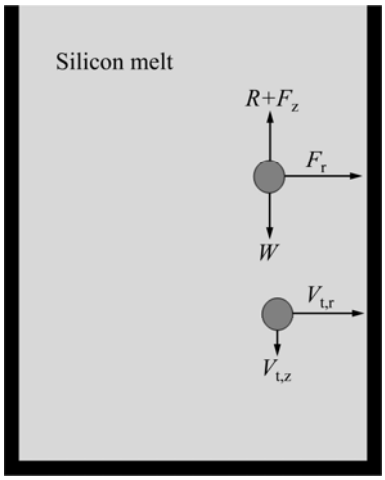

Fig. 4 Schematic view of different forces acting on nonconductive particle suspending in liquid metal and related migration velocities

The drag force acting on the inclusion by the melt in vertical orientation is given by

$$\boldsymbol{R}=-\frac{1}{2}\rho_{\mathrm{f}}\cdot\frac{\pi d_{\mathrm{p}}^2}{4}C_{\mathrm{D}}\cdot|\boldsymbol{v}|\boldsymbol{v} \tag{5}$$

where $\boldsymbol{R}$ is the drag force exerted on a unit volume of the inclusion; C_{D} is the drag coefficient; $\boldsymbol{v}$ is the movement velocity in the vertical orientation of the inclusion and ρ_{f} is the density of the melt.

The relationship between the moving velocity of the inclusion and prescribed forces is shown in Eq. (6):

$$\boldsymbol{W}+\boldsymbol{R}+\boldsymbol{F}_{\mathrm{p}}=(\rho_{\mathrm{p}}-\rho_{\mathrm{f}})\boldsymbol{g}V_{\mathrm{p}}-\frac{1}{2}\rho_{\mathrm{f}}\cdot\frac{\pi d_{\mathrm{p}}^2}{4}\cdot C_{\mathrm{D}}\cdot|\boldsymbol{v}|\boldsymbol{v}-\frac{3}{4}\frac{\pi d_{\mathrm{p}}^3}{6}\cdot\boldsymbol{J}\times\boldsymbol{B}=\frac{\pi d_{\mathrm{p}}^3}{6}\rho_{\mathrm{p}}\frac{\mathrm{d}\boldsymbol{v}}{\mathrm{d}t} \tag{6}$$

where $\boldsymbol{W}$ is the effective gravity of the inclusion in the melt; d$\boldsymbol{v}$/dt is the acceleration of the inclusion; $\boldsymbol{g}$ is the gravity acceleration, and ρ_{p} is the density of inclusion. The viscous resistance of the inclusion increases as the velocity increases. In the absence of electromagnetic forces and when the net force exerted by the gravity of the inclusion and the viscous resistance of the inclusion are in balance, the velocity of the inclusion reaches the terminal velocity (v_{t}).

$$v_{\mathrm{t}}=\sqrt{\frac{\pi d_{\mathrm{p}}(\rho_{\mathrm{p}}-\rho_{\mathrm{f}})}{6C_{\mathrm{D}}\rho}} \tag{7}$$

Assuming Reynolds number for small inclusion in micron size range is less than 1, C_{D} in Eq. (5) is taken to be 24/Re which leads to the following relation:

$$v_{\mathrm{t}}=\frac{d_{\mathrm{p}}^2(\rho_{\mathrm{p}}-\rho_{\mathrm{f}})\boldsymbol{g}}{18\nu} \tag{8}$$

Considering the effect of electromagnetic forces on the particles, the terminal velocity is calculated based on the following equation:

$$\boldsymbol{v}_{\mathrm{t}}=\frac{d_{\mathrm{p}}^2\left[(\rho_{\mathrm{p}}-\rho_{\mathrm{f}})\boldsymbol{g}+\frac{3}{4}\boldsymbol{J}\times\boldsymbol{B}\right]}{18\nu} \tag{9}$$

In Eq. (9), ν represents viscosity of the liquid metal. Since the electromagnetic forces are stronger than gravity close to the crucible side walls. The first term in Eq. (9) can be neglected in these zones and the particles velocity then are calculated as follows:

$$\boldsymbol{v}_{\mathrm{t}}=\frac{d_{\mathrm{p}}^2}{24\nu}\cdot\boldsymbol{J}\times\boldsymbol{B} \tag{10}$$

Due to strong stirring of the liquid metal caused by the electromagnetic forces, it is reasonable to assume that the melt is completely mixed, resulting in a homogeneous particle concentration. Using this assumption the conservation equation for the inclusions in the melt is given by Eq. (11). This equation expresses time evolution of the particle concentration in the bulk of melt. The non-conductive particles are removed from the bulk of melt as they reach in vicinity of the crucible wall, within the skin depth δ (~4.33 mm) due to the existence of prescribed electromagnetic forces; they are accumulated on the wall. The rate at which the particles are accumulated on the crucible wall is considered the particle removal rate from the bulk of melt.

$$V\frac{\mathrm{d}C}{\mathrm{d}t}=-[A_{\mathrm{W}}(\boldsymbol{v}_{\mathrm{t}}\boldsymbol{e}_{\mathrm{r}})+A_{\mathrm{B}}(\boldsymbol{v}_{\mathrm{t}}\boldsymbol{e}_z)]C \tag{11}$$

where V is volume of the melt; C is content of SiC particles; A_{W} is area of side wall and A_{B} is area of crucible bottom wall; $\boldsymbol{e}_{\mathrm{r}}$ is the radial unit vector; $\boldsymbol{e}_z$ is the vertical unit vector. The first term in the parenthesis is the average radial velocity at the side wall and the second term in the parenthesis represents the average vertical velocity at the bottom.

4.1 Governing equations on fluid flows

The Lavers method is used as the basis to calculate the electromagnetic fields in the induction furnace. Using this method magnetic flux density, Joule heat, and the different components of the electromagnetic force in liquid metal are obtained. Using the standard k–ε turbulence model, the governing transport equations are as follows:

$$\nabla\boldsymbol{u}=0 \tag{12}$$

$$\rho(\boldsymbol{u}\cdot\nabla)\boldsymbol{u}=\nabla\cdot[-pI+(\nu+\nu_{\mathrm{t}})(\nabla\boldsymbol{u}+(\nabla\boldsymbol{u})^{\mathrm{T}})]+\boldsymbol{F} \quad (13)$$

$$\rho\boldsymbol{u}\cdot\nabla k=\nabla\cdot\left[\left(\nu+\frac{\nu_{\mathrm{t}}}{\sigma_k}\right)\nabla k\right]+\nu_{\mathrm{t}}\nabla\boldsymbol{u}:[\nabla\boldsymbol{u}+(\nabla\boldsymbol{u})^{\mathrm{T}}]-\rho\varepsilon \quad (14)$$

$$\rho\boldsymbol{u}\cdot\nabla\varepsilon=\nabla\cdot\left[\left(\nu+\frac{\nu_{\mathrm{t}}}{\sigma_\varepsilon}\right)\nabla\varepsilon\right]+$$

$$C_{1\varepsilon}\varepsilon\nu_{\mathrm{t}}\nabla\boldsymbol{u}:[\nabla\boldsymbol{u}+(\nabla\boldsymbol{u})^{\mathrm{T}}]/k-C_{2\varepsilon}\rho\varepsilon^2/k \quad (15)$$

where I is identity or unit matrix; ε is turbulent dissipation rate; k is turbulent kinetic energy.

Turbulent viscosity and the model parameters are as follows:

$$\nu_{\mathrm{t}}=C_{\mu}k^2/\varepsilon \quad (16)$$

$$C_{\mu}=0.09, C_{1\varepsilon}=1.44, C_{2\varepsilon}=1.92, \sigma_k=1, \sigma_\varepsilon=1.3 \quad (17)$$

where C_{μ} is the turbulent model constant.

Finally, the boundary conditions are required to complete the definition of the flow problem. We have specified zero velocity wall functions on the solid surfaces and zero shear on the free surface. Furthermore, the k and ε are set as zero on the solid surfaces and their gradients are stipulated to be zero on the free surfaces.

4.2 Geometry of induction furnace

A 3D CFD model of the induction furnace was developed. The furnace geometry and its electrical parameters have been selected based on the laboratory scale induction furnace used in experimental work. The geometrical and electrical properties of the induction furnace are presented in Table 2 and Fig. 5 shows a cross section of the furnace used in modelling.

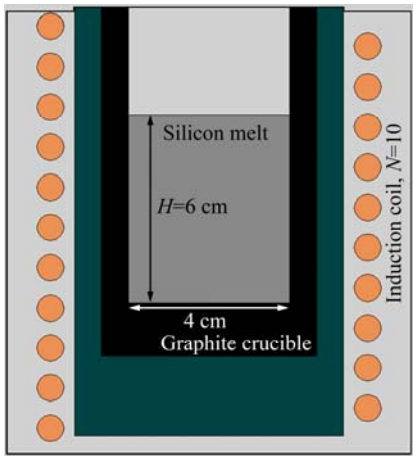

Fig. 5 Geometries of induction furnace used in CFD modelling of fluid flows in silicon melt

5 Results

The governing equations for the fluid flows are solved using COMSOL Multiphysics 3.5a. The results of the CFD model then are used as the input parameters in the prescribed classical models of particle removal from the melt. The obtained results from both the modelling and experimental works are described in the following.

5.1 Modelling results

The results of the CFD model show that due to the fairly high electrical conductivity of liquid silicon, the induced current in the melt is very high. The vectors of induced current density at different heights in the melt are shown in Fig. 6. It can be seen that the induced current has higher values in the regions very close to the crucible walls comparing with the other zones of the melt.

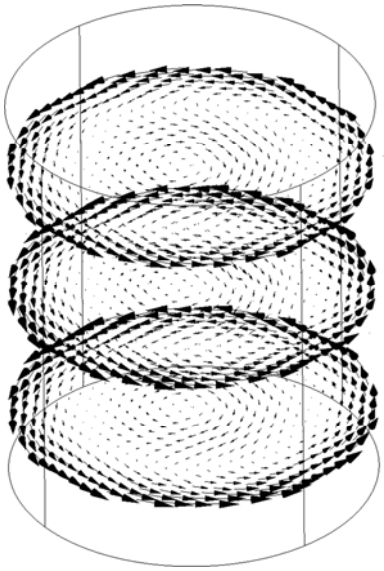

Fig. 6 Vectors of induced current density in silicon melt at three different levels

Interaction between the induced current in the melt and the magnetic field created due to current pass through the induction coil, leads to the generation of electromagnetic Lorentz forces in the melt. The vectors of Lorentz forces in a vertical cross section of the crucible are presented in Fig. 7. It is clearly seen from Fig. 7 that the electromagnetic forces are very strong near the crucible walls. This phenomenon causes effective separation of the inclusion particles from the melt when the particles get close to the crucible walls.

Due to existence of the electromagnetic forces, the melt flow inside the crucible shows a complex turbulent flow pattern which assures good mixing in the liquid silicon. Figure 8 represents the velocity pattern of the melt in the central plane of the crucible. It is seen from Fig. 8 that the silicon melt flows upwards in the central part of the crucible and moves downwards in the zones close to the walls. The resulted melt flow pattern shows that there is a very good stirring and therefore complete

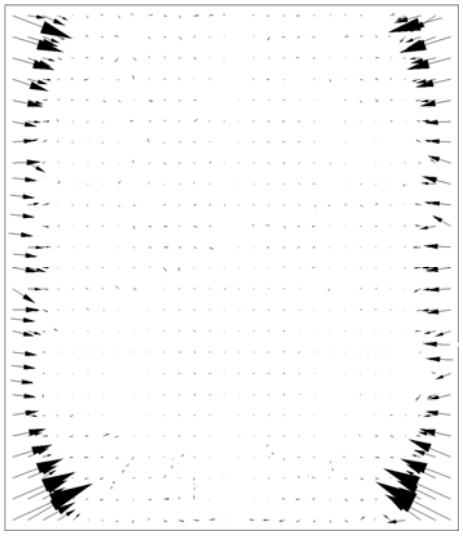

Fig. 7 Vectors of electromagnetic Lorentz forces in central vertical cross section of crucible

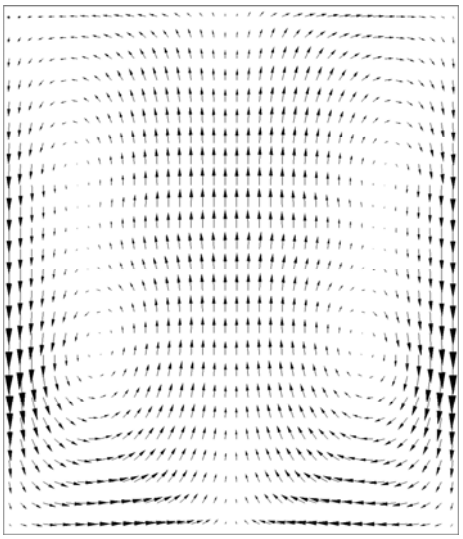

Fig. 8 Velocity flow pattern in central vertical cross section of crucible showing stirring of silicon melt under effect of electromagnetic forces

mixing in the melt. This means that it is very likely that the SiC particles can reach the crucible wall.

The results of the model show that as the result of electromagnetic forces the nonconductive particles are pushed away from the bulk of silicon melt and they are accumulated on the crucible side and bottom wall. Therefore, the particle concentration in the melt decreases to a lower amount as the separation process proceeds. Figure 9 shows the prediction of model for evolution of the content of the SiC particles in the melt for 600 s after start of separation.

The results show that the particle separation rate is very high as the process begins and it slows down to a much lower rate as time goes on. It could be predicted that the bigger particles are separated from the melt much faster than the smaller ones. This phenomenon is clearly seen from Fig. 10 which shows the change in the size distribution of the inclusion particles in the silicon melt as the separation process continues.

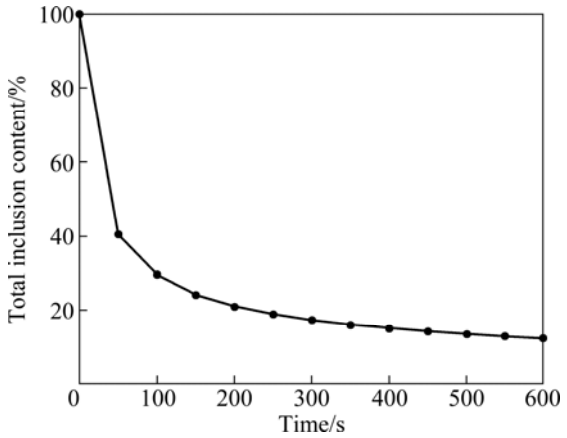

Fig. 9 Result of model showing evolution of total content of SiC particles in silicon melt for 600 s after start of separation process

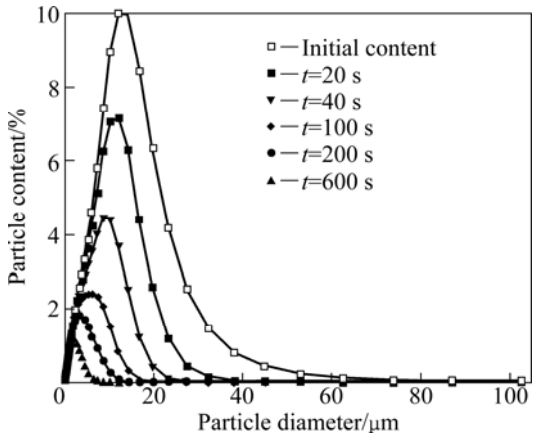

Fig. 10 Size distribution of SiC particles in melt with separation process proceeding

The removal efficiency for the size group of i among the SiC particles is defined as follows [13]:

$$\eta_i = \frac{C_{i0} - C_i}{C_{i0}} \tag{18}$$

where C_{i0} represents the initial content of particle size i and C_i shows the same parameter as the separation process proceeds. The removal efficiency is a factor which determines how effective the electromagnetic separation for each particle size is. The removal efficiency as a function of particles size is shown in Fig. 11. It shows that the smaller the particles size, the lower the removal efficiency.

The changes in unified content of each individual SiC particle as a function of time are presented in Fig. 12. It shows that the content of smaller particles in the melt

decreases very slowly which again shows the difficulty in getting rid of this range of particles.

5.2 Experimental results

The micro-structural studies indicate that the SiC particles are located on the crucible walls. Particles content on the crucible side wall is absolutely more than the bottom wall. This shows that the particle removal has happened due to the effect of electromagnetic forces than particle sedimentation because of the gravity force. Very few or none SiC particles could be observed in the middle of crucible. No large SiC particle was observed in the middle of crucible and away from the wall. It is worth mentioning that a thin SiC layer is formed on the crucible wall through the contact of molten silicon with graphite, and this type of silicon is also seen in some areas in the graphite due to the penetration of the liquid silicon to the open pores. This SiC is distinguishable easily with the suspended SiC particles added to the silicon. These results can be observed for all the samples in Figs. 13 and 14. It can be seen that the thickness of the apparent SiC aggregation area on the crucible wall varies with the total SiC content. No difference between samples B and C was observed, meaning that the dispersion of SiC particles into the melt is probably similar or it does not matter for the applied melting time.

The metallography study supports the model prediction and the effect of the electromagnetic forces under the induction melting on the SiC separation. Obviously, the SiC particles are separated through the induction melting from the melt and pushed to the walls. It is worth noting that the content of SiC particles on the side wall is much higher comparing with the bottom wall

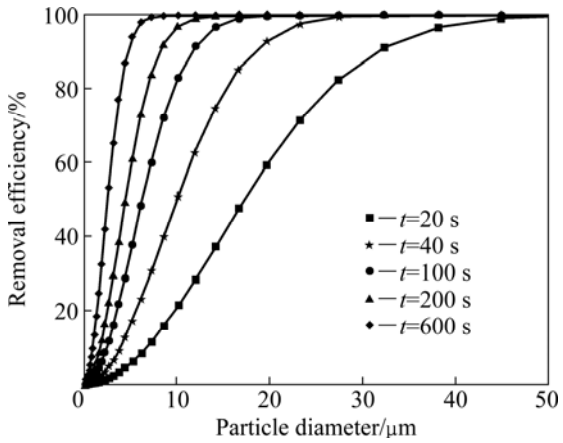

Fig. 11 Particle removal efficiency based on particle size showing bigger SiC particles more likely to be separated from silicon melt in a shorter period of time

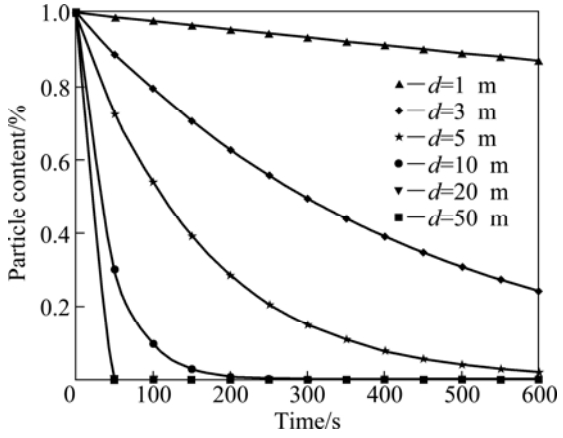

Fig. 12 Evolution in content of each individual particles size showing limitation of electromagnetic separation method in removing very small particles

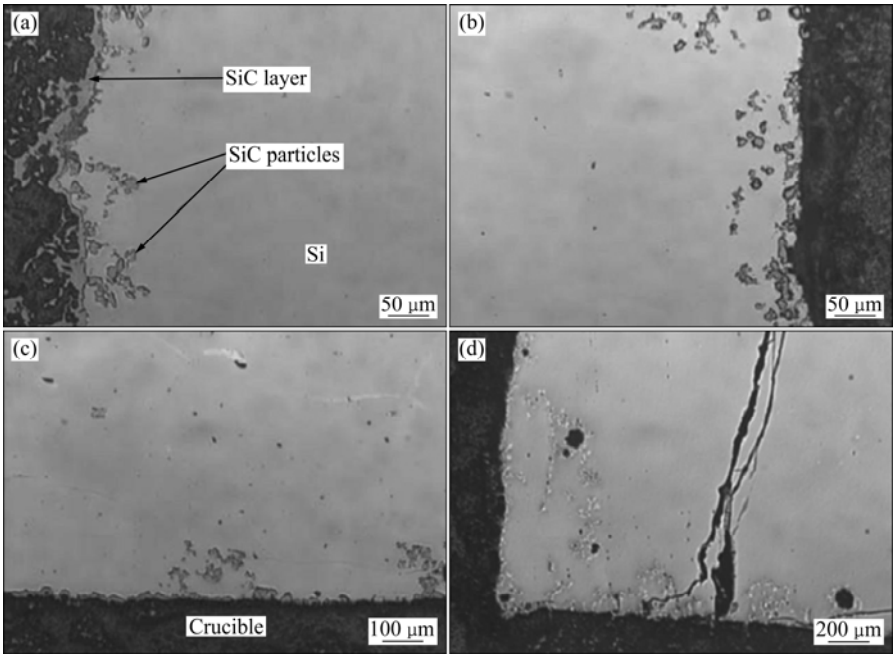

Fig. 13 Microscopy images from different positions of silicon/crucible interfacial area in experiment A

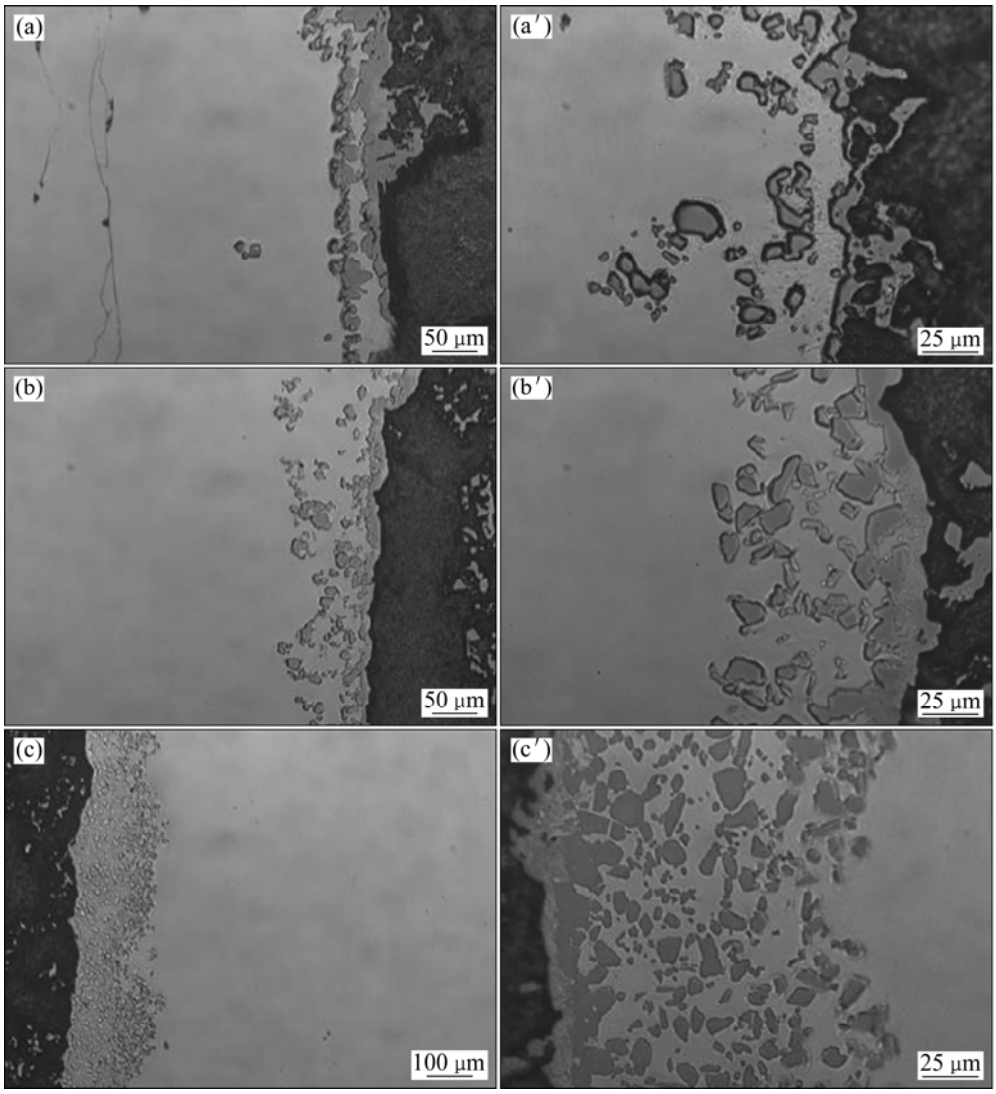

Fig. 14 Microscopy images from silicon/graphite crucible interfacial area in experiments B (a,a′), C (b,b′) and D (c,c′)

of crucible. This indicates more efficient particle separation due to the electromagnetic forces comparing with gravity force.

6 Conclusions

1) Feasibility of removing the nonconductive SiC particles from silicon melt using the electromagnetic separation method was studied. A conceptual model of the electromagnetic separation process was developed. The model is made of a combination of classical models of inclusion removal and a CFD model for calculation of electromagnetic forces, melt flows etc in a laboratory scale induction furnace. The results show that it is possible to use this method for purification of silicon melt from nonconductive inclusions.

2) The experimental studies for different conditions prove the validity of the model and the results show that this method can be successfully applied for purification of silicon melt from the SiC particles. The particle content on the crucible side wall is significantly more than the crucible bottom wall, which proves that the particle separation is mainly because of electromagnetic forces but not gravity force.

3) It should be mentioned that in the experiments the melt holding time is continued for 12 min while our model which has been made based on complete mixing assumption, predicts faster inclusion removal rate. Therefore, it is recommended that the experiments with shorter holding time for the melt will be performed in future.

References

[1] MÜHLBAUER A, DIERS V, WALTHER A. Removal of C/SiC from liquid silicon by directional solidification [J]. Journal of Crystal Growth, 1991, 108(1−2): 41−52.

[2] TANIGUCHI S, YOSHIKAWA N, TAKAHASHI K. Application of

EPM to the separation of inclusions particles from liquid metal [C]//Proceedings of the 15th Riga and 6th Pamir conference on fundamental and applied MHD. Riga, 2005: 55−63.

[3] LEENOV D, KOLIN A. Theory of electromagnetophoresis I: Magnetohydrodynamic forces experienced by spherical and symmetrically oriented cylindrical particles [J]. Journal of Chemical Physics, 1954, 22(4): 683−688.

[4] MARTY P, ALEMANY A. Metallurgical application of magnetohydrodynamics [C]//Proceedings of the Symposium of IUTAM. London, 1984: 245−259.

[5] TANIGUCHI S, BRIMACOMBE J K. Application of pinch force to the separation of inclusion particles from liquid steel [J]. ISIJ International, 1994, 34(9): 722−731.

[6] ALEMANY A, ARGOUS J P, BARLET J, IVANES M, MOREAU R, POINSOT S. French Patent No.80400 4430, 1980.

[7] TANIGUCHI S, KIKUCHI A. Removal of nonmetallic inclusion from liquid metal by AC-electromagnetic force [C]//Proceedings of the 3rd International Symposium on Electromagnetic Processing of Materials, EPM2000, Nagoya, 2000: 315−320.

[8] EL-KADDAH N, PATEL A D, NATARAJAN T T. The electromagnetic filtration of molten aluminum using an induced-current separator [J]. JOM, 1995, 47(5): 46−49.

[9] SHU D, SUN B, LI K, XU Z, ZHOU Y. Effect of secondary flow on the electromagnetic separation of inclusions from aluminum melt in a square channel by a solenoid [J]. ISIJ International, 2002, 42(11): 1241−1250.

[10] LI K, WANG J, SHU D, LI T, SUN B, ZHOU Y. Theoretical and experimental investigation of aluminum melt cleaning using alternating electromagnetic field [J]. Materials Letter, 2002, 56: 215−220.

[11] HJELLMING L N, WALKER J S. Melt motion in a Czochralski crystal puller with an axial magnetic field: isothermal motion [J]. Journal of Fluid Mechanics, 1986, 164: 237−273.

[12] SCHEI A, TUSET J, TVEIT H. Production of high silicon alloys [M]. Trondheim: Tapir forlag, 1998: 363.

[13] TAKAHASHI K, TANIGUCHI S. Electromagnetic separation of nonmetallic inclusion from liquid metal by imposition of high frequency magnetic field [J]. ISIJ International, 2003, 43(6): 820−827.

采用高频磁场去除太阳能级硅熔体中的 SiC 粒子

Mehdi KADKHODABEIGI[1], Jafar SAFARIAN[1], Halvard TVEIT[1], Merete TANGSTAD[1], Stein Tore JOHANSEN[2]

1. Department of Materials Science and Engineering, Norwegian University of Science and Technology (NTNU), P.O. Box 7491, Trondheim, Norway;
2. SINTEF Materials and Chemistry, Flow technology group, P.O. Box 7465, Trondheim, Norway

摘　要：高质量硅材料在光伏太阳能和电子设备中具有重要应用，然而原料中的非金属颗粒和金属杂质严重影响其电学性能和力学性能。由于 SiC 粒子会降低光伏电池的力学性能并导致分流问题，因此在制备太阳能电池之前必须将这些杂质从硅材料中去除。利用磁场去除液态金属中的非金属杂质是制备高纯金属的一项尖端技术。利用该方法去除冶金级硅材料中的 SiC 粒子，并结合杂质去除经典模型和计算流体力学对熔体中粒子浓度和分离效率进行计算。为检验该方法的有效性，采用感应炉进行多次实验。结果表明：该方法能有效去除非金属杂质，提纯硅熔体，且实验结果与模型的预测结果相符。

关键词：SiC 粒子；电磁分离；太阳能级硅；光电管；计算流体学；非金属颗粒；金属杂质

(Edited by LI Xiang-qun)